

# Jet Effects on Coflow Jet Airfoil Performance

Ge-Cheng Zha,\* Wei Gao,† and Craig D. Paxton‡  
University of Miami, Coral Gables, Florida 33124

DOI: 10.2514/1.23995

A control volume analysis is presented in this paper to analyze the jet effect on the coflow jet airfoil with injection and suction and on the airfoil with injection only. The formulations to calculate the duct's reactionary forces that must be included for the lift and drag calculation are given. The computational fluid dynamics solutions based on the Reynolds-averaged Navier–Stokes model are used to provide the breakdowns of lift and drag contributions from the airfoil surface force integral and jet duct's reactionary forces. The results are compared with experiment for validation. The duct reactionary forces are also validated with the result of a 3-D computational fluid dynamics calculation of the complete airfoil with jet ducts and wind tunnel walls. The study indicates that the suction occurring on the airfoil suction surface of the coflow jet airfoil is more beneficial than the suction occurring through the engine inlet such as the airfoil with injection only. For the airfoil with injection only, the drag actually acted on the aircraft, or the equivalent drag, is significantly larger than the drag measured by the wind tunnel balance due to the ram drag and captured area drag when the jet is drawn from the freestream. For a coflow jet airfoil, the drag measured by the wind tunnel balance is the actual 2-D drag that the aircraft will experience. A coflow jet airfoil does not have the ram drag and captured area drag. For a coflow jet airfoil, the suction penalty is offset by the significant circulation enhancement. The coflow jet airfoil with both injection and suction yields stronger mixing, larger circulation, more filled wake, higher stall angle of attack, less drag, and lower energy expenditure.

## Nomenclature

$A$	= area
$C_D$	= drag coefficient
$C_L$	= lift coefficient
$C_\mu$	= momentum coefficient
$D$	= drag
$E$	= endurance
$\mathbf{F}$	= resultant force
$k$	= turbulent kinetic energy
$L$	= lift
$\dot{m}$	= mass flow rate
$P$	= power required
$P_t$	= total pressure
$p$	= static pressure
$\mathbf{R}$	= force from airfoil surface integral
$\mathbf{R}'$	= reactionary force of $\mathbf{R}$
$S$	= wing span area ( $b \times \text{chord}$ )
$u, v, w$	= velocity components in $x, y,$ and $z$ direction
$\mathbf{V}$	= velocity vector
$y^+$	= nondimensional length scale for turbulent boundary layer
$\alpha$	= angle of attack
$\gamma$	= ratio of specific heats; suction coefficient: 1 suction on; 2 suction off
$\epsilon$	= turbulent dissipation rate
$\theta$	= angle between slot surface and the line normal to chord
$\rho$	= density

$\infty$  = freestream

## Subscripts

$e$	= control volume exit
ei	= engine inlet
$j$	= jet injection
1	= injection slot
2	= suction slot
$\infty$	= freestream

## I. Introduction

FLOW control (FC) is a promising means to significantly improve airfoil performance and has attracted more and more attention lately as the technology for future high-performance, high-efficiency aircraft [1–7]. Zha et al. have recently developed a new airfoil flow control concept using coflow jet (CFJ) [8–11], which drastically increases lift, stall margin, and drag reduction.

The coflow jet airfoil is to open an injection slot near the leading edge and a suction slot near the trailing edge on the airfoil suction surface as shown in Fig. 1. A high-energy tangential jet in the same direction of the main flow is injected near the leading edge and the same amount of mass flow is sucked in near the trailing edge. The turbulent shear layer between the main flow and the jet causes strong turbulence diffusion and mixing under severe adverse pressure gradient, which enhances lateral transport of energy from the jet to main flow and allows the main flow to overcome severe adverse pressure gradient and remain attached at high angle of attack (AoA). The high-energy jet induces a large circulation, which generates high lift and reduces drag or generates thrust due to strong leading-edge suction. The CFJ airfoil is a zero net mass flux flow control, which minimizes the power consumption.

In [8,9], an overview of different flow control methods is given. Compared with the circulation control (CC) airfoil [12,13] as shown in the sketch of Fig. 2, the working mechanism of CFJ airfoil is different. A CC airfoil relies on large leading edge (LE) or trailing edge (TE) to have the Coanda effect and enhance circulation. The large TE or LE hence generate large drag during cruise. The CFJ airfoil relies on the wall jet mixing with the main flow to energize the main flow and overcome the adverse pressure gradient so that the flow can induce high circulation and remain attached at high AoA. The CC airfoil dumps away the jet mass flow, which is a considerable

Presented as Paper 0102 at the 44th Aerospace Sciences Meeting and Exhibit Conference, Reno, NV, 8–12 January 2006; received 17 March 2006; revision received 28 November 2006; accepted for publication 7 February 2007. Copyright © 2007 by G.-C. Zha, W. Gao and C. D. Paxton. Published by the American Institute of Aeronautics and Astronautics, Inc., with permission. Copies of this paper may be made for personal or internal use, on condition that the copier pay the \$10.00 per-copy fee to the Copyright Clearance Center, Inc., 222 Rosewood Drive, Danvers, MA 01923; include the code 0001-1452/07 \$10.00 in correspondence with the CCC.

\*Associate Professor, Department of Mechanical and Aerospace Engineering; gzha@miami.edu. Member AIAA.

†Graduate Student, Department of Mechanical and Aerospace Engineering.

‡Graduate Student, Department of Mechanical and Aerospace Engineering; currently Boeing Company, Phantom Works, Huntsville, AL.

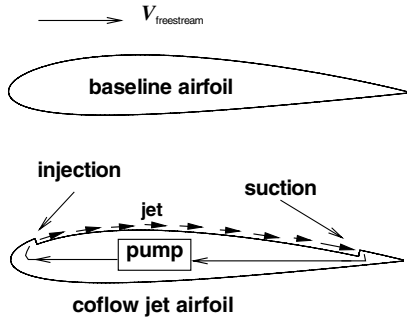


Fig. 1 Baseline NACA2415 and CFJ airfoil.

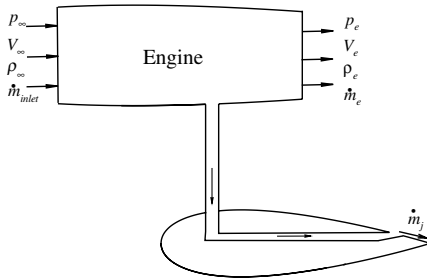


Fig. 2 Sketch of an airfoil with injection only integrated with a propulsion system.

penalty to the propulsion system. The CFJ airfoil has a zero net mass flux and significantly reduces the penalty to power consumption. A CC airfoil without LE injection may reduce stall margin even though it increases the lift [14].

Compared with the synthetic jet flow control, the enhancement of airfoil performance by the CFJ airfoil is much more drastic because the interaction of the synthetic jet (either generated by acoustic wave or plasma) with the main flow is weak [8,9,15]. A CFJ airfoil simultaneously achieves three drastic effects at low energy expenditure: lift enhancement, stall margin increase, and drag reduction. The mission analysis conducted in [8] indicates a significant improvement of fuel consumption reduction, increase of range and endurance, and a drastic reduction of takeoff and landing distance.

The turbulent mixing between the jet and main flow to transfer energy from the jet to the main flow is the fundamental working principle of CFJ airfoil [8]. The injection slot should be located as close to the leading edge as possible, but should be located downstream of the suction peak. This is to make use of the adverse pressure gradient after the suction peak to enhance the wall jet mixing with the main flow [16]. In [9,10], the injection slot size effect is studied experimentally. It is found that the smaller injection slot has higher stall AoA and hence high maximum lift. The energy expenditure of the airfoil with smaller injection slot is significantly less than that of the airfoil with large injection slot size. This indicates that there is a great potential to optimize the CFJ airfoil performance such as reducing the amount of jet mass flow with optimum configuration or pulsed jet, etc.

The coflow jet airfoil concept suggested by Zha et al. [8–10] appears to have the following advantages: 1) very effective to enhance lift and suppress separation; 2) drastically reduces drag and can achieve very high 2-D  $C_L/C_D$  at low AoA (infinity when  $D \leq 0$ , which is a thrust), and very high lift and drag at high AoA (takeoff and landing); 3) significantly increases AoA operating range and stall margin; 4) has very low energy expenditure; 5) can be applied to any airfoil, thick or thin; 6) can be used for whole flying mission instead of only takeoff and landing; 7) can be used for low- and high-speed aircraft; and 8) easy implementation with no moving parts.

The CFJ airfoil concept is new and hence many issues of the working mechanism need to be further studied. For example, a question that is often asked is, compared with the CC airfoil that has

no suction, will the streamwise suction of the CFJ airfoil hurt the airfoil performance? This question is based on the conception that a streamwise injection will generate a thrust due to its momentum and hence reduce the drag, whereas a streamwise suction will do the opposite. However, this question is somewhat misleading and has forgotten the fact that, for any flow control process, as long as an injection is used, a suction is necessary based on the law of mass conservation. The valid question then should be as follows: Where and how the suction occurs will be more beneficial, the suction occurring on the airfoil suction surface such as a CFJ airfoil (see Fig. 1), or the suction occurring on the engine such as a CC airfoil (see Fig. 2)? This paper is to answer this important question.

The objective of this paper is to conduct a control volume analysis to analyze the effect of the injection and suction jet. The 2-D and 3-D computational fluid dynamics (CFD) simulations are used to provide the detailed data breakdowns. The experimental results are used to validate the results. The study in this paper indicates that for the airfoil with injection only, the equivalent drag, which is the drag actually acted on the aircraft, is significantly larger than the drag measured by the wind tunnel balance because of the ram and captured area drag when the jet is drawn from the freestream. For a CFJ airfoil, the drag measured by the wind tunnel balance is the actual 2-D drag that the aircraft will experience. The CFJ airfoil does not have the ram drag and captured area drag. The measured performance of the CFJ airfoil has already included the suction penalty, which is offset by the significant circulation enhancement. The CFJ airfoil with both injection and suction yields stronger mixing, larger circulation, more filled wake, higher stall angle of attack, less drag, and more efficient energy expenditure.

In this paper, when the term “CFJ airfoil” is used, it means the standard CFJ airfoil with both injection and suction.

## II. Control Volume Analysis

### A. CFJ Airfoil

Take a control volume **abcdefghia** surrounding a CFJ airfoil as shown in Fig. 3 with the following assumptions: the freestream flow comes into the control volume from the inlet on the left and exits the control volume from the outlet on the right. The freestream flow is perpendicular to the inlet and outlet boundaries. The upper and lower boundaries are parallel to the freestream flow. The pressures at the control volume boundaries are uniform and are equal to the freestream pressure. A jet is injected from slot 1 and the same amount of mass flow is drawn into the airfoil at slot 2. The flow is steady state inside the control volume.

Let  $\mathbf{R}_x$  and  $\mathbf{R}_y$  represent the components of the pressure and shear stress integral acted by the *airfoil surface* on the control volume in  $x$  and  $y$  directions.

The momentum equation on the control volume **abcdefghia** gives

$$\sum \mathbf{F} = \iint_s \rho \mathbf{V} \cdot \mathbf{dS} \cdot \mathbf{V} \quad (1)$$

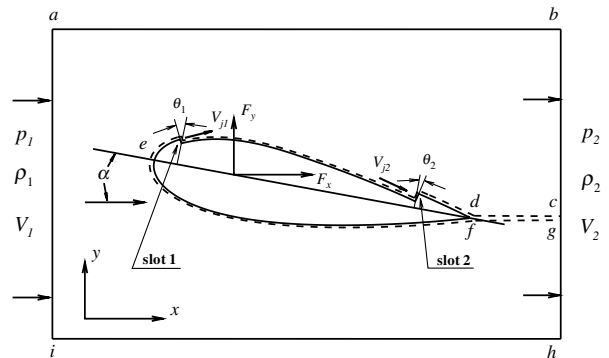


Fig. 3 Control volume for a CFJ airfoil.

The left-hand side of Eq. (1) is the resultant force acting on the control volume. The right-hand side of the equation is the momentum variation across the control volume boundary.

Equation (1) in  $x$  direction is

$$\begin{aligned} & -p_e A_e + p_\infty A_\infty + (p_{j1} A_{j1})_x - (p_{j2} A_{j2})_x + R_x \\ & = \int_h^b \rho V_e dy V_e - \int_i^a \rho V_\infty dy V_\infty - \dot{m}_{j1} u_{j1} + \dot{m}_{j2} u_{j2} \end{aligned} \quad (2)$$

Because  $p_e = p_\infty$  and  $A_e = A_\infty$ , the first two items on the left-hand side of Eq. (2) are canceled out.

Let  $F_{xcfj}$  stand for the reactionary force generated by the jet ducts in  $x$  direction, then

$$\begin{aligned} F_{xcfj} &= [\dot{m}_{j1} u_{j1} + (p_{j1} A_{j1})_x] - \gamma [\dot{m}_{j2} u_{j2} + (p_{j2} A_{j2})_x] \\ &= (\dot{m}_j V_{j1} + p_{j1} A_{j1}) * \cos(\theta_1 - \alpha) \\ &\quad - \gamma (\dot{m}_j V_{j2} + p_{j2} A_{j2}) * \cos(\theta_2 + \alpha) \end{aligned} \quad (3)$$

For the CFJ0025-065-196 airfoil [9] analyzed in this paper,  $\theta_1 = 25.86$  deg,  $\theta_2 = 14.31$  deg, and  $V_j$  is the jet velocity. Equation (3) is obtained based on the momentum equation by creating a control volume inside the airfoil between the injection and suction slots.

The total drag, which is the one measured by the wind tunnel balance, is the summation of the airfoil surface drag and the reactionary force in drag direction generated by the injection and suction ducts. Based on the Newton's third law that a force and its reactionary force have the same magnitude and opposite direction, the drag  $D$  is then

$$D = -(R_x + F_{xcfj}) = R'_x - F_{xcfj} \quad (4)$$

$R'_x$  is the CFJ airfoil surface pressure and shear stress integral in  $x$  direction.

$$R'_x = -R_x \quad (5)$$

Substituting Eqs. (2) and (3) into Eq. (4), then the total drag is

$$D = R'_x - F_{xcfj} = \int_i^a \rho V_\infty dy V_\infty - \int_h^b \rho V_e dy V_e \quad (6)$$

For a CFJ airfoil, the injection and suction have the same mass flow rate. Hence, the mass conservation gives

$$\dot{m}_{j1} = \dot{m}_{j2} \quad (7)$$

and

$$\int_i^a \rho V_\infty dy = \int_h^b \rho V_e dy \quad (8)$$

Equation (6) then becomes

$$D = R'_x - F_{xcfj} = \int_h^b \rho V_e (V_\infty - V_e) dy \quad (9)$$

or

$$C_D = C_{Drake} \quad (10)$$

The following conclusions can be drawn from the preceding equations:

1) For a CFJ airfoil, the total drag is the drag measured by the wind tunnel balance, and is equal to the drag calculated by the wake rake measurement. This is the same conclusion as that for a conventional airfoil with no flow control or an airfoil using flow control with zero net mass flux.

2) The injection has the effect of reducing drag due to the jet thrust [see Eqs. (3) and (4)].

3) The suction has the effect of increasing drag [see Eqs. (3) and (4)].

The lift measured by the wind tunnel balance is

$$L = R'_y - F_{ycfj} \quad (11)$$

where  $R'_y$  is the  $y$ -direction component of the surface pressure and shear stress integral, which is primarily induced by the circulation.  $F_{ycfj}$  is the jet duct's reactionary force component in  $y$  direction:

$$\begin{aligned} F_{ycfj} &= [\dot{m}_{j1} v_{j1} + (p_{j1} A_{j1})_y] - \gamma [\dot{m}_{j2} v_{j2} + (p_{j2} A_{j2})_y] \\ &= (\dot{m}_j V_{j1} + p_{j1} A_{j1}) * \sin(\theta_1 - \alpha) \\ &\quad + \gamma (\dot{m}_j V_{j2} + p_{j2} A_{j2}) * \sin(\theta_2 + \alpha) \end{aligned} \quad (12)$$

Equations (11) and (12) indicate that 1) the injection has the effect of reducing lift when  $v_{j1} > 0$ , increasing lift when  $v_{j1} < 0$ ; 2) the suction almost always has the effect of decreasing lift.

If only based on the thrust generated by the momentum, the injection is always beneficial and the suction always has a penalty. However, both the drag and lift are mostly determined by  $R'_x$  and  $R'_y$ , the surface drag and surface lift. The numerical simulation indicates that the suction has the effect to reduce  $R'_x$  and increase  $R'_y$ . The benefit of the suction outweighs the penalty, and hence the airfoil achieves a net performance gain.

## B. Airfoil with Injection Jet Only

A sketch of a injection only airfoil integrated with an aircraft engine is shown in Fig. 2. The jet mass flow is sucked in at the engine inlet from freestream and injected on the airfoil.

In a wind tunnel test, when an airfoil has injection jet only such as the CC airfoil, the jet mass flow is usually drawn from outside of the wind tunnel. The jet mass flow is added into the total wind tunnel exit mass flow. The mass conservation hence gives

$$\int_i^a \rho V_\infty dy = \int_h^b \rho V_e dy - \dot{m}_j \quad (13)$$

Because there is no suction, the measured drag in a wind tunnel test based on Eq. (6) becomes

$$\begin{aligned} D_{\text{windtunnel}} &= R'_x - [\dot{m}_j u_j + (p_j A_j)_x] = R'_x - (\dot{m}_j V_j + p_j A_j) \\ &\quad * \cos(\theta - \alpha) = \int_h^b \rho V_e (V_\infty - V_e) dy - m_j V_\infty \end{aligned} \quad (14)$$

or

$$C_{D\text{windtunnel}} = C_{Drake} - C_\mu \frac{V_\infty}{V_j} \quad (15)$$

where  $C_\mu$  is defined as

$$C_\mu = \frac{\dot{m}_j V_j}{0.5 \rho_\infty U_\infty^2 S} \quad (16)$$

That is, for an airfoil with jet injection only, the drag measured by the balance in a wind tunnel is equal to the drag calculated based on the wake rake measurement minus  $m_j V_\infty$ . This is the same conclusion as that given in [17] and adopted in [18].

However, in reality, when the airfoil with jet injection only is used in an aircraft, there must be an air flow source for the injection. Usually, the engine draws the air from the freestream and blows it on the wing surface as shown in Fig. 2.

Assume that the wing jet flow source is from the engine inlet, the actual drag that the airfoil will experience can be still determined by Eqs. (2–4). The only difference is that the suction parameters will be those at engine inlet. The actual drag with the suction effect is also often called equivalent drag [18]:

$$D_{\text{equiv}} = R'_x - [\dot{m}_j u_j + (p_j A_j)_x] + \dot{m}_j V_{ei} + p_{ei} A_{jei} \quad (17)$$

Based on Eq. (14), the equivalent drag is

$$D_{\text{equiv}} = D_{\text{windtunnel}} + \dot{m}_j V_{\text{ei}} + p_{\text{ei}} A_{j_{\text{ei}}} \quad (18)$$

$A_{j_{\text{ei}}}$  is the captured area to draw the jet mass flow from freestream. The drag due to the term  $\dot{m}_j V_{\text{ei}}$  is the ram drag. The drag due to the term  $p_{\text{ei}} A_{j_{\text{ei}}}$  is the captured area drag.

Based on mass conservation,

$$\rho_{\text{ei}} V_{\text{ei}} A_{j_{\text{ei}}} = \dot{m}_j \quad (19)$$

we then have

$$p_{\text{ei}} A_{j_{\text{ei}}} = \frac{\dot{m}_j V_{\text{ei}}}{\gamma M_{\text{ei}}^2} \quad (20)$$

Then Eq. (18) becomes

$$\begin{aligned} C_{D_{\text{equiv}}} &= C_{D_{\text{windtunnel}}} + C_{\mu} \frac{V_{\text{ei}}}{V_j} + C_{\mu} \frac{V_{\text{ei}}}{V_j \gamma M_{\text{ei}}^2} \\ &= C_{D_{\text{windtunnel}}} + C_{\mu} \frac{V_{\text{ei}}}{V_j} \left( 1 + \frac{1}{\gamma M_{\text{ei}}^2} \right) \end{aligned} \quad (21)$$

Equation (21) indicates that, when the Mach number at engine inlet is increased, the ram drag is also increased due to the higher velocity, and the captured area drag is decreased due to the reduced captured area for the jet. The captured area drag is significantly larger than the ram drag if the flow at engine inlet is subsonic. During a flight mission, the flow parameters at the engine inlet may or may not be equal to the freestream parameters. For example, at the starting point to takeoff, the freestream velocity is zero, but the velocity at the engine inlet is far greater than zero to satisfy the engine mass flow requirement to generate the required thrust. During a flight mission, when the mass flow rate required by the engine is equal to the mass flow rate captured by the straight flow tube going into the engine inlet, the freestream flow parameters will be equal to the flow parameters at engine inlet. The drag increase for the airfoil with injection only due to the ram and captured area drag can be also considered as the loss of thrust [8].

If assume  $V_{\text{ei}} = V_{\infty}$ , based on Eqs. (15) and (21), we have

$$C_{D_{\text{equiv}}} = C_{D_{\text{drake}}} + C_{\mu} \frac{V_{\text{ei}}}{V_j \gamma M_{\text{ei}}^2} \quad (22)$$

The lift for the airfoil with injection only is

$$\begin{aligned} L &= R'_y - [\dot{m}_j v_{j1} + (p_{j1} A_{j1})_y] \\ &= R'_y - (\dot{m}_j V_{j1} + p_{j1} A_{j1}) * \sin(\theta_1 - \alpha) \end{aligned} \quad (23)$$

The jet suction from the freestream has no component in  $y$  direction. Hence the lift here is the same as the lift measured by the wind tunnel balance.

The equivalent drag formulation used in [18,19] is different from the one derived in this paper. The assumption used in [18,19] is that the jet is taken from a large reservoir. As a reference, the formulation is given as follows [18]:

$$C_{D_{\text{equiv}}} = C_{D_{\text{windtunnel}}} + C_{\mu} \frac{V_{\infty}}{V_j} + C_{\mu} \frac{V_j}{2V_{\infty}} \quad (24)$$

Using Eq. (15),

$$C_{D_{\text{equiv}}} = C_{D_{\text{drake}}} + C_{\mu} \frac{V_j}{2V_{\infty}} \quad (25)$$

### III. Jet Effect on Airfoil Performance

Compare Eqs. (9) and (14); one of the important differences between the CFJ airfoil and the airfoil with injection only (e.g., a CC airfoil) is that for the airfoil with injection only, the drag actually acted on the aircraft, the equivalent drag, could be significantly larger than the drag measured by the wind tunnel balance because of the ram and captured area drag. For a CFJ airfoil, the drag measured by the

wind tunnel balance is the actual 2-D drag that the aircraft will experience. The CFJ airfoil does not have the ram drag and captured area drag.

The reason for this difference is that for a 2-D CFJ airfoil, the jet mass conservation is satisfied by the injection and suction. The jet injection and suction effect is already included in the measured lift and drag in a wind tunnel. For a 2-D injection only airfoil such as a CC airfoil, the jet mass flow conservation is not satisfied because there is no jet flow source inside the airfoil. However, this does not prevent the measurement of a 2-D airfoil with injection only in a wind tunnel because the jet flow is usually drawn into the airfoil from the side, which is perpendicular to the streamwise plane. The suction hence will have no effect on the drag and lift.

For a CFJ airfoil, both the injection and suction occur on the suction surface of the airfoil. Compared with an airfoil with injection only, the CFJ airfoil will have the jet attached more strongly due to the suction. This will induce a stronger circulation and have a higher stall AoA than the airfoil with injection only. The distance between the injection and suction with the adverse pressure gradient provides an intensive mixing process, which fills the wake and reduces drag. Based on Eq. (9), the shallower the wake profile, the smaller the drag of the CFJ airfoil. If the wake has reversed velocity deficit, a thrust is generated. The CFJ airfoil will usually have a significantly lower drag than the airfoil with injection only due to the stronger mixing.

The power required to pump the coflow jet for CFJ airfoil based on Eq. (3) is

$$\begin{aligned} P_{\text{cfj}} &= V_{\infty} F_{\text{xcfj}} = V_{\infty} [(\dot{m}_j V_{j1} + p_{j1} A_{j1}) * \cos(\theta_1 - \alpha) \\ &\quad - (\dot{m}_j V_{j2} + p_{j2} A_{j2}) * \cos(\theta_2 + \alpha)] \end{aligned} \quad (26)$$

The power required to pump the jet flow for the airfoil with injection only is

$$\begin{aligned} P_{\text{inj only}} &= V_{\infty} F_{\text{xinj only}} = V_{\infty} [(\dot{m}_j V_{j1} + p_{j1} A_{j1}) * \cos(\theta_1 - \alpha) \\ &\quad - (\dot{m}_j V_{\text{ei}} + p_{\text{ei}} A_{j_{\text{ei}}})] \end{aligned} \quad (27)$$

The CFD results to be shown later indicate that the  $P_{\text{inj only}}$  is significantly greater than  $P_{\text{cfj}}$ .

### IV. CFD Solver

The Fluent CFD software is used in this research to calculate the 2-D and 3-D CFJ airfoil flows. The governing equations are the Reynolds-averaged 3-D compressible Navier–Stokes (RANS) equations. The pressure-based second-order upwind scheme is used to evaluate the inviscid flux and central differencing is used for the viscous terms. The  $k-\epsilon$  turbulence model with integration to the wall and pressure gradient effect is employed. The  $y_1^+$  is in the order of 1. The  $k-\epsilon$  model is selected due to its capability of taking into account of turbulent boundary layer history effect by solving the complete transport equations of  $k$  and  $\epsilon$ . The  $k-\epsilon$  model is more capable than algebraic models to predict the separated flows, which occur when the airfoil stalls at high AoA.

The full turbulent boundary layer assumption is used and is consistent with the tripped boundary layer in the experiments. Mesh refinement study is conducted for a few selected points to ensure that the solutions are mesh size independent. Because the CFD solutions are obtained from the steady-state calculations based on the RANS model, the unsteady details of the shear layer mixing entrainment and large coherent vortex structures are not able to be captured.

The wind tunnel walls are included in the CFD simulation to consider the wind tunnel wall effect. The total pressure and total temperature are given at the wind tunnel inlet as the boundary conditions. The static pressure at wind tunnel exit is iterated to make the wind tunnel inlet Mach number match the experimental value. The total pressure and total temperature are also given at the injection duct inlet as the boundary conditions. The injection total pressure is iterated to match the experimental momentum coefficient. The static pressure at the suction duct entrance is iterated to match the injection jet mass flow rate.

As mentioned, several layers iterations are needed to achieve a converged CFJ airfoil solution at a certain AoA. The calculation is thus CPU intensive, in particular for 3-D cases. The 2-D CFJ airfoil calculation is therefore very desirable. The control volume analysis in this paper not only gives an insight of the CFJ airfoil working principle, but also provides the formulation to calculate the lift and drag to include the effect of the jet duct's reactionary forces.

## V. Results and Discussion

### A. Geometry

Figure shows the baseline airfoil, NACA0025, the CFJ airfoil, and the airfoil with injection only. The NACA0025 airfoil was selected as the baseline airfoil due to its large thickness to facilitate implementation of coflow jet, internal ducts, and instrumentation. The chord length of the airfoil is 0.1527 m and the span is 0.3 m. The coflow jet airfoils are named using the following convention: CFJ4dig-INJ-SUC, where 4dig is the same as NACA 4 digit convention, INJ is replaced by the percentage of the injection slot size to the chord length, and SUC is replaced by the percentage of the suction slot size to the chord length. For example, the CFJ0025-065-196 airfoil in Fig. 4 has the injection slot height of 0.65% of the chord and the suction slot height of 1.96% of the chord.

The suction surface shape is a downward translation of the portion of the original suction surface between the injection and suction slot. The injection and suction slot are located at 7.11% and 83.18% of the chord from the leading edge. The slot faces are normal to the suction surface to make the jet tangential to main flow. In the experiment, the high-pressure flow is injected into the high pressure cavity and then goes through a metallic foam to make the injection jet uniform. The CFD simulations take the downstream interface of the foam as the injection inlet.

To compare the performance of a CFJ airfoil with injection suction and the airfoil with injection only, the CFJ0025-065-000 airfoil is created with no suction slot as shown in Fig. 4. The injection slot is exactly the same as that of the CFJ0025-065-196 airfoil. The suction surface has the same shape as that of the baseline NACA0025 airfoil. The last 3 digits "000" of the CFJ0025-065-000 airfoil means that the airfoil has no suction slot.

### B. CFJ Airfoil with Both Injection and Suction

Figure 5 is the zoomed 2-D mesh near the CFJ0025-065-196 airfoil. The structured mesh is used around the airfoil and unstructured mesh is used in the region away from the airfoil where

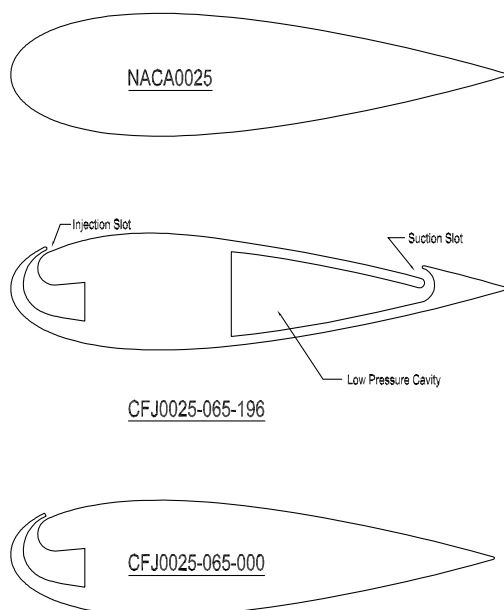


Fig. 4 Airfoil section of the baseline airfoil of NACA0025, CFJ0025-065-196 airfoil, and CFJ0025-065-000 airfoil.

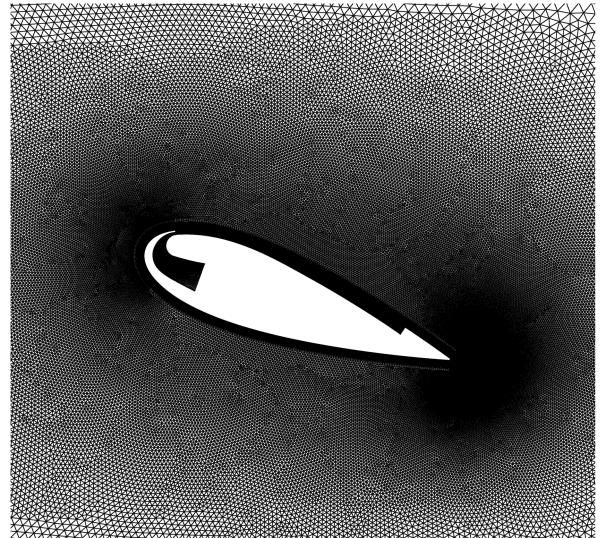


Fig. 5 2-D mesh for CFD calculation of the CFJ0025-065-196 airfoil.

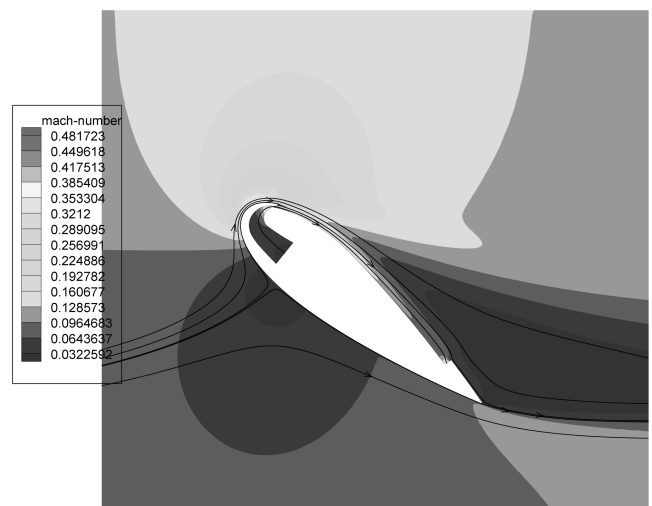


Fig. 6 Computed Mach number contours with streamlines for CFJ0025-065-196 airfoil at AoA = 39 deg.

the flow gradient is small. The total number of cells is 170,000. The freestream Mach number is 0.1 and the Reynolds number based on chord is 380,000. The flow is assumed normal to the injection duct inlet. The suction duct is only simulated with an entrance opening because the flow inside the suction duct has little effect on the flow outside of the suction duct. Simulation of the injection duct gives a more realistic injection mixing effect when the jet enters into the main flow. Figure 6 is the Mach number contours and streamlines of the CFJ0025-065-196 airfoil at AoA = 39 deg. The flow is attached and is consistent with the experiment [9].

Figure 7 is the computed lift coefficient compared with the experiment. The solid square and triangle symbols are the experimental results of the CFJ airfoil and the baseline airfoil. In the experiment, the baseline airfoil stalls at AoA = 19 deg with  $C_{L_{max}} = 1.57$ , and the CFJ airfoil stalls at AoA = 44 deg with  $C_{L_{max}}$  of 5.04. The CFJ airfoil has increased maximum lift by 220% and stall margin by 153%. The predicted baseline airfoil lift (solid circle symbols) agrees fairly well with the experiment (solid triangle symbols), except that the stall AoA is about 3 deg higher than the experiment.

The open square symbol is the lift coefficient calculated by the surface integral of pressure and shear stress. This is the lift generated primarily by circulation, which is the  $R'_y$  given in Eq. (11) and is higher than the measured lift. The solid diamond symbols are the lift with the contribution made by the injection duct reactionary force,

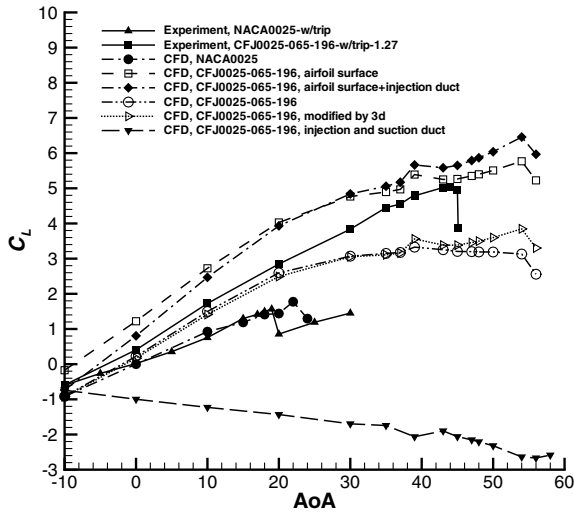


Fig. 7 Computed lift coefficient compared with experiment at different AoA.

the first term of Eq. (12). It can be seen that the injection jet does not have a large effect on lift. It slightly reduces the lift at low AoA ( $v_j \geq 0$ ) and slightly increases the lift at high AoA ( $v_j \leq 0$ ). When the suction effect [second term in Eq. (12)] is added, the final lift is reduced significantly as shown by the open circle symbols.

Obviously, the final lift computed based on Eq. (11) agrees fairly well with the experiment up to AoA = 20 deg. When the AoA is greater than 20 deg, the computation underpredicts the lift significantly. The large discrepancy may be due to the inherent unsteadiness of the mixing process at high AoA under large adverse pressure gradient. The RANS model used is not able to accurately capture the unsteady mixing process, which could have large vortex structure such as the coherent vortices due to the jet dissimilarity and Görtler vortices due to the surface curvature. The very bottom curve with solid downward triangle symbols in Fig. 7 is the calculated total lift contribution generated by the jet ducts based on Eq. (12). It means that the lift reduction amount due to the jet ducts is large and is mainly made by the suction jet.

Figure 8 is the computed drag coefficient compared with the experiment. The two lines with solid square and triangle symbols are the measured drag coefficient of the CFJ airfoil and the baseline airfoil. The CFJ airfoil has the measured drag lower than that of the baseline airfoil before the baseline airfoil stalls. In the region of zero angle of attack, the CFJ airfoil has negative drag, that is, thrust. The CFD (solid circle symbols) predicts the baseline airfoil drag

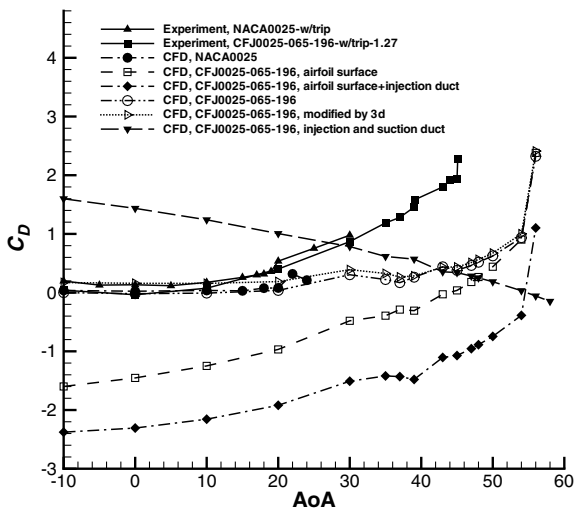


Fig. 8 Computed drag coefficient compared with experiment at different AoA.

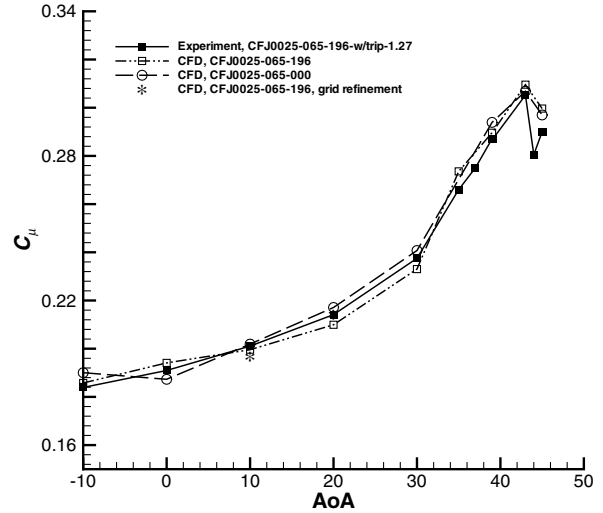


Fig. 9 Computed momentum coefficient compared with experiment at different AoA.

coefficient quite well when AoA ≤ 10 deg. When AoA ≥ 10 deg, the predicted drag coefficient remains flat for the baseline airfoil, whereas the measured baseline airfoil drag coefficient increases. The discrepancy between the predicted and measured drag is hence large at high AoA.

The open square symbol in Fig. 8 is the drag coefficient determined by the surface integral of pressure and shear stress, the  $R'_x$  in Eq. (4). It is significantly lower than the measured drag and has negative value up to nearly AoA = 50 deg. The negative drag is primarily due to the strong leading-edge suction, which results in a thrust due to the resultant pressure force. The injection further reduces the drag due to the jet momentum as shown by the solid diamond symbols and is calculated based on Eq. (3). When the suction duct reactionary force is added based on Eqs. (3) and (4), the drag is brought very close to the measured drag as shown by the open circle symbols in Fig. 8. This shows that the control volume analysis indeed gives a good quantitative correction of the drag. Similar to the lift prediction, the CFJ airfoil drag is predicted quite well at low AoA. At high AoA, the CFJ airfoil drag prediction is similar to the baseline case and is fairly flat, most probably due to the inadequate turbulence simulation by the RANS model. The dash line curve on the top with the solid downward triangle symbols is the total drag force due to the jet ducts calculated based on Eq. (3). It can be seen that the jet ducts, in particular the suction duct, have a significant contribution to the drag.

Figure 9 is the computed momentum coefficient compared with the experimental results. They agree well and the maximum difference is less than 2%.

To validate the duct's reactionary forces computed based on Eqs. (3) and (12), a 3-D case with the airfoil, wind tunnel walls, and the experimental injection and suction ducts are simulated at zero angle of attack. Figure 10 shows the 3-D mesh and Fig. 11 shows the 3-D streamlines released from the injection duct, which indicates that the flowfield has a good two-dimensionality. For the surface force integral calculation of the injection duct, the duct inlet is treated as a fictitious wall so that the pressure on the wall can be counted as in the experiment. The total 3-D resultant force generated by the ducts then can be obtained. The total drag and lift can be calculated based on Eqs. (4) and (11). However, the  $F_{x_{cfj}}$  and  $F_{y_{cfj}}$  are determined by the 3-D duct surface integral forces instead of Eqs. (3) and (12) for this 3-D case. An assumption is made that the resultant force generated by the ducts has constant magnitude at different AoA and is always along the chordwise direction. The calculated lift and drag coefficients at different AoA are then plotted in Figs. 7 and 8 as the dot lines with open right-triangle symbols. They agree amazingly well with the results using the 2-D control volume correction.

The 3-D results support two conclusions: 1) the results of the 2-D control volume analysis provide accurate duct reactionary forces for

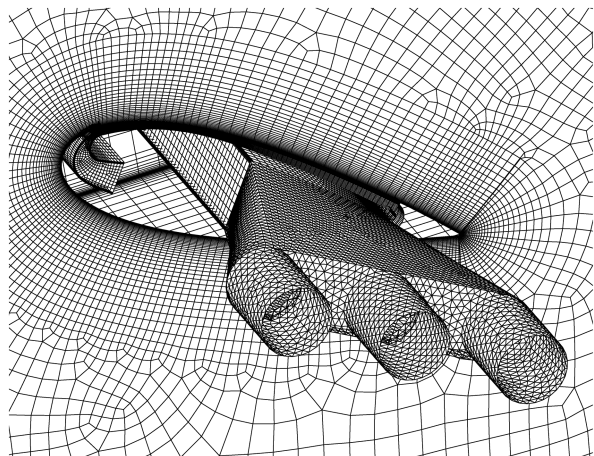


Fig. 10 3-D mesh for CFD calculation of the CFJ0025-065-196 airfoil with injection and suction ducts.

the lift and drag; 2) the assumption that the duct’s resultant force has constant magnitude at different AoA along the chordwise direction is reasonable. The rationale for this assumption is that the duct internal force is not affected much by the airfoil external main flowfield at different AoA.

C. Airfoil with Injection Only

To compare the performance of a CFJ airfoil with injection suction and the airfoil with injection only, the CFJ0025-065-000 airfoil shown in Fig. 4 is calculated using the same CFD solver and mesh size. The injection momentum coefficient is approximately the same as that of the CFJ0025-065-196 airfoil as shown in Fig. 9. The maximum deviation of the computed  $C_{\mu}$  from the experiment is less than 2%.

Figure 12 is the comparison of the lift coefficient for the CFJ0025-065-000 airfoil and CFJ0025-065-196 airfoil. The computed total lift coefficients have included the jet reactionary force effect determined by Eqs. (11) and (23). Both CFJ0025-065-000 and CFJ0025-065-196 airfoils have higher lift coefficient and stall AoA than the baseline airfoil (see Fig. 7). The computed lift coefficient shows that the CFJ0025-065-196 airfoil has higher lift and stall AoA than the CFJ0025-065-000 airfoil. Figure 12 also demonstrates that the lift contribution due to circulation,  $R'_y$ , for the CFJ0025-065-196 airfoil (solid triangle) is substantially larger than that of the CFJ0025-065-000 airfoil (solid diamond).

Figure 13 is the comparison of the drag coefficient for the CFJ0025-065-000 and CFJ0025-065-196 airfoils. The computed results indicate that the CFJ0025-065-196 airfoil (open square

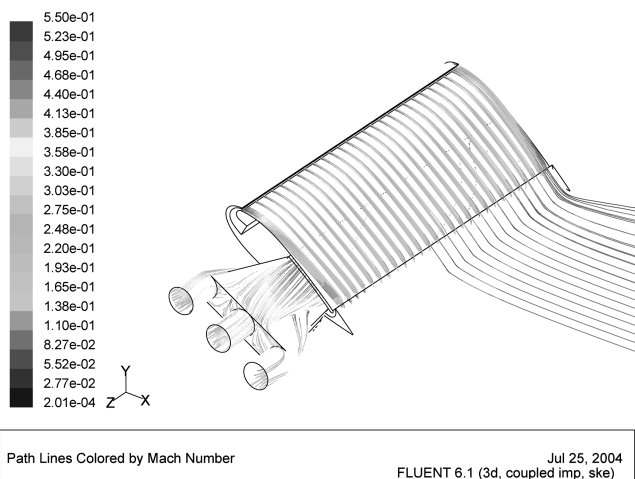


Fig. 11 Streamlines released from the injection jet of the 3-D calculation.

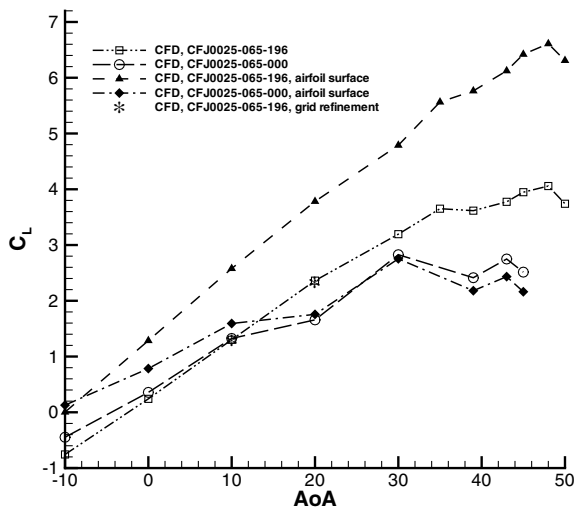


Fig. 12 Comparison of the computed lift coefficient for the CFJ airfoil and the airfoil with injection only.

symbols) has lower 2-D drag than the CFJ0025-065-000 airfoil (open circle symbols), in particular at high AoA.

The equivalent drag of the CFJ0025-065-000 airfoil is significantly higher than the drag of the CFJ0025-065-196 airfoil calculated by either Eq. (21) (open triangle symbols) given in this paper or Eq. (25) (solid circle symbols) given in [18]. The equivalent drag calculated based on Eq. (21) is substantially larger than that determined by Eq. (25) [18]. For CFJ0025-065-196 airfoil, the equivalent drag is the same as the measured drag and hence is significantly lower than the equivalent drag of the CFJ0025-065-000 airfoil. The lower drag means lower energy expenditure. Figure 13 shows that the drag contribution due to circulation,  $R'_x$ , for the CFJ0025-065-196 airfoil (solid triangle) is all negative (thrust) and the counterpart of the CFJ0025-065-000 airfoil is all positive (solid diamond).

The mesh refinement study is conducted for the flows at AoA = 10 and 20 deg. The mesh size around the airfoil is doubled. The lift, drag, and momentum coefficients of the refined mesh are shown in Figs. 12, 13, and 9 with the \* symbol. The lift and drag are virtually the same. The  $C_{\mu}$  variation is less than 1%, which is in the uncertainty range. The mesh refinement study indicates that the results based on the baseline mesh are independent of the mesh size.

The results at AoA = 20 deg are used for comparison of the details for the CFJ airfoil and the airfoil with injection only. Figures 14 and 15 are the Mach contours of the CFJ0025-065-000

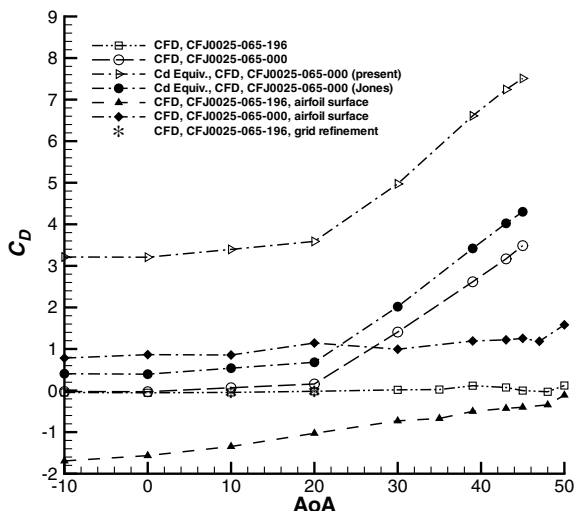


Fig. 13 Comparison of the computed drag coefficient for the CFJ airfoil and the airfoil with injection only.

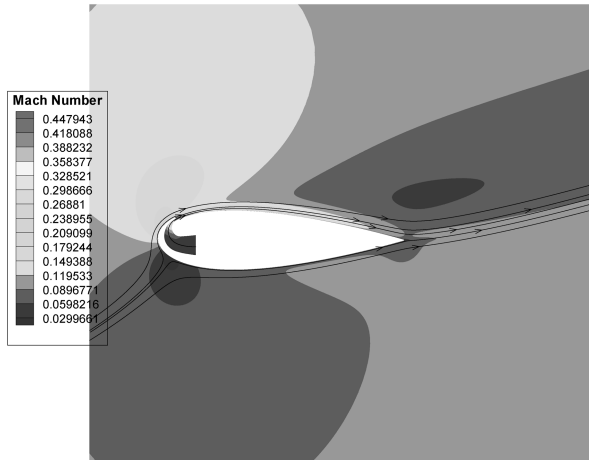


Fig. 14 Mach number contours with streamlines for CFJ0025-065-000 airfoil with injection only at AoA = 20 deg.

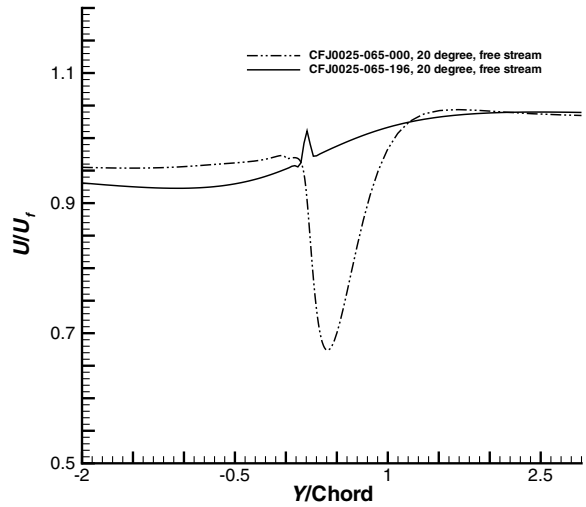


Fig. 16 Wake profiles of the CFJ airfoil and the airfoil with injection only.

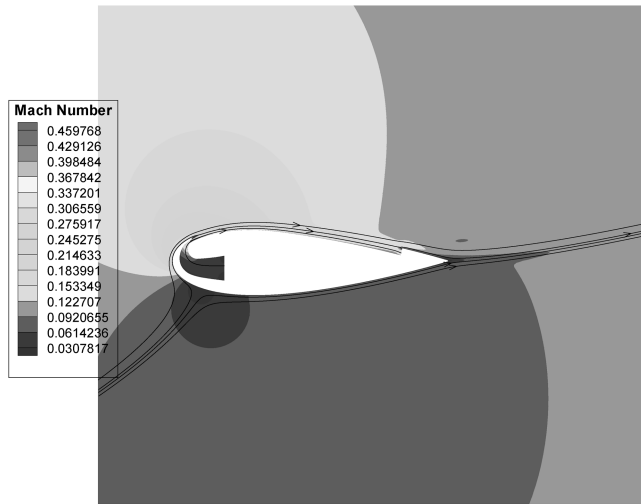


Fig. 15 Mach number contours with streamlines for CFJ0025-065-196 airfoil at AoA = 20 deg.

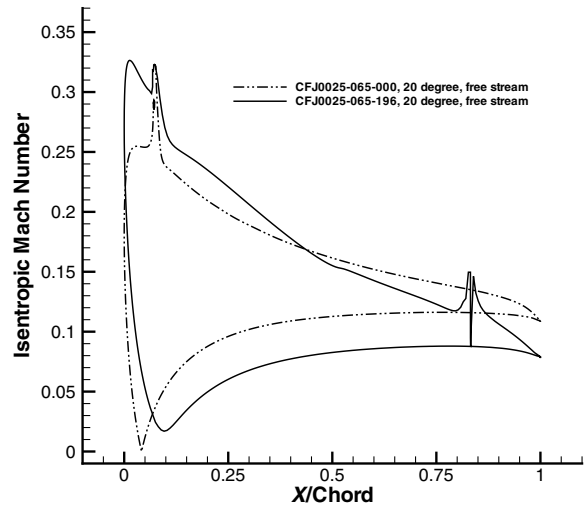


Fig. 17 Airfoil surface isentropic Mach number distributions of the CFJ airfoil and the airfoil with injection only.

airfoil and CFJ0025-065-196 airfoil. The following are the observations:

1) The CFJ0025-065-000 airfoil has a large wake region with low momentum (deep color region). The CFJ0025-065-196 airfoil basically has no wake. This indicates that the CFJ airfoil with both injection and suction has stronger mixing and energy transfer than the airfoil with injection only. The main flow of the CFJ airfoil is more energized by the jet with both injection and suction.

2) The stagnation point of the CFJ0025-065-196 airfoil is more downstream than that of the CFJ0025-065-000 airfoil. This indicates that the circulation induced by the CFJ airfoil with both injection and suction is greater than that of the airfoil with injection only. The higher circulation also yields higher leading-edge peak Mach number.

Figure 16 is the wake profiles of the CFJ0025-065-196 airfoil and CFJ0025-065-000 airfoil. Even though both airfoils have the same injection jet location and jet strength, the CFJ0025-065-196 airfoil has a reversed velocity deficit, whereas the CFJ0025-065-000 airfoil has a deep wake. This means that the jet suction enhances the mixing and fills the wake more than the airfoil without jet suction. There is more energy transferring between the jet and the main flow when both injection and suction are used.

Figure 17 is the surface isentropic Mach number for CFJ0025-065-196 airfoil and CFJ0025-065-000 airfoil. It can be seen that the surface loading, or the circulation, of the CFJ0025-065-196 airfoil is much larger than that of the CFJ0025-065-000 airfoil. The leading-edge suction peak Mach number of the CFJ0025-065-196 airfoil is

higher and the stagnation point is more downstream. It can be seen that the injection location is located downstream of the peak Mach number to make use of the adverse pressure gradient to enhance mixing [16].

Tables 1–3 give the quantitative comparison of the performance of the CFJ0025-065-196 and CFJ0025-065-000 airfoils at AoA = 20 deg. The flow parameters at the engine inlet are assumed to be equal to the freestream flow parameters.

Table 1 compares the computed lift coefficients and their breakdowns for the CFJ0025-065-196 and CFJ0025-065-000 airfoils. The momentum coefficients of the two airfoils are about the same. Table 1 indicates that the lift coefficient of the CFJ0025-065-196 airfoil is 42% higher than that of the CFJ0025-065-000 airfoil. The primary contribution is from the lift generated by circulation,  $R'_y$ , which is 115% higher than that of the CFJ0025-065-000 airfoil. The injection jet generates about the same lift reduction for both airfoil. The suction generates a lift reduction for the CFJ0025-065-196

Table 1 Comparison of lift coefficient and its breakdowns for the two CFJ airfoils at AoA = 20 deg

Airfoil	$C_\mu$	$C_L$	$R'_y$	$F_y$ inj.	$F_y$ suc.
CFJ0025-065-196	0.21	2.36	3.78	-0.096	-1.33
CFJ0025-065-000	0.217	1.66	1.76	-0.1	0



**Table 2 Comparison of drag coefficient and its breakdowns for the two CFJ airfoils at AoA = 20 deg**

Airfoil	$C_D$	$R'_x$	$F_x$ inj.	$F_x$ suc.	$C_D$ equiv
CFJ0025-065-196	-0.018	-1.03	-0.93	1.94	-0.018
CFJ0025-065-000	0.17	1.14	-0.97	3.43	3.6 (present), 0.68 (Jones [18])

**Table 3 Comparison of the power required to pump the jet for the two CFJ airfoils at AoA = 20 deg**

Airfoil	Power required
CFJ0025-065-196	1
CFJ0025-065-000	2.4

airfoil. For CFJ0025-065-000 airfoil, the suction is from the freestream and hence has no lift component. Even though the suction of the CFJ airfoil has the effect of reducing lift, the total lift is still higher than that of the CFJ0025-065-000 airfoil because of the higher circulation.

Table 2 compares the drag coefficients and their breakdowns for the CFJ0025-065-196 and CFJ0025-065-000 airfoils at AoA = 20 deg. Table 2 indicates that the 2-D drag (first column) coefficients of the CFJ0025-065-196 airfoil is lower than that of the CFJ0025-065-000 airfoil. For CFJ0025-065-196 airfoil, the surface force integral,  $R'_x$ , generates a large thrust (negative drag). This is because the high circulation induces a strong leading-edge suction with low pressure, which results in a forward thrust. The suction of the CFJ airfoil induces a large drag. However, the suction penalty is offset by the large negative drag generated by the circulation,  $R'_x$ , of the CFJ airfoil.

On the contrary, for the CFJ0025-065-000 airfoil, the surface force integral generates a large drag as a conventional airfoil. The injection reduces drag for both airfoils due to the injection jet thrust. If the 2-D drags of the two airfoils are considered as not too much different, the equivalent drag of the CFJ0025-065-000 airfoil is significantly larger than that of the CFJ0025-065-196 airfoil. The equivalent drag is the drag that the aircraft will be actually experienced. For the CFJ0025-065-000 airfoil, the equivalent drag calculated by Eq. (21) given in the present paper is significantly larger than that calculated by the Eq. (25) given in [18]. However, even if based on the Eq. (25) given in [18], the equivalent drag of the airfoil with injection only is still much larger than the 2-D drag of the CFJ0025-065-000 airfoil, and is also substantially larger than the drag of the CFJ airfoil.

The power required to pump the jet for the CFJ0025-065-196 and CFJ0025-065-000 airfoils at AoA = 20 deg are calculated based on Eqs. (26) and (27) and are given in Table 3. The power required to pump the CFJ0025-065-000 airfoil with injection only is 2.4 times that required to pump the CFJ0025-065-196 airfoil.

In conclusion, the suction of the CFJ airfoil does come with a effect of reducing lift and increasing drag. The fact is that a suction is necessary for any flow control process that uses a jet injection. However, the suction of a CFJ airfoil also brings the benefit of enhancing the circulation. Comparing the CFJ airfoil with injection suction, the airfoil with injection only and the baseline noncontrolled airfoil, the benefit of the CFJ airfoil suction significantly outweighs the penalty and yields a net performance gain for the CFJ airfoil. The CFJ airfoil has higher lift, higher stall margin, lower drag, and lower power consumed. The drag measured in the wind tunnel for the CFJ airfoil is the actual drag that is acted on an aircraft. The performance penalty of a CFJ airfoil due to the suction is already counted in the wind tunnel measurement.

## VI. Conclusions

The control volume analysis of a CFJ airfoil provides the lift and drag breakdowns contributed by its surface force integral and the reactionary forces generated by the jet ducts. These formulations are necessary to calculate the duct reactionary forces to be included for 2-D CFJ airfoil calculation. The lift and drag calculated by CFD using

$k-\epsilon$  turbulence model are compared well with the experiment when the AoA is less than 20 deg. At high AoA, both the lift and drag are significantly underpredicted. The large discrepancy at high AoA may be primarily due to the inadequacy of a RANS turbulence model to simulate the unsteady jet-mixing process. The duct reactionary forces are also validated by a 3-D CFD calculation of the complete airfoil with jet ducts and wind tunnel wall. The reactionary forces computed by the control volume formulations agree well with the results of the 3-D computation.

A suction process of the jet is necessary for all flow control methods as long as they use flow injection. This is governed by the law of mass conservation. The comparative study between a CFJ airfoil with injection and suction and a airfoil with the injection only is conducted. The study indicates that the suction occurring on the airfoil suction surface such as the CFJ airfoil is much more beneficial than the suction occurring through the engine inlet such as the airfoil with injection only. For the airfoil with injection only, the drag actually acted on the aircraft, the equivalent drag, is significantly larger than the drag measured by the wind tunnel balance because of the ram and captured area drag when the jet is drawn from the freestream. For a CFJ airfoil, the drag measured by the wind tunnel balance is the actual 2-D drag that the aircraft will experience. The CFJ airfoil does not have the ram drag and captured area drag. For a CFJ airfoil, the benefit of the suction outweighs the penalty due to the significant circulation enhancement. The CFJ airfoil with both injection and suction yields stronger mixing, larger circulation, more filled wake, higher stall angle of attack, less drag, and lower energy expenditure.

## References

- [1] Sellers, W. L. I., Singer, B. A., and Leavitt, L. D., "Aerodynamics for Revolutionary Air Vehicles," AIAA Paper 2004-3785, June 2003.
- [2] Gad-el Hak, M., "Flow Control: The Future," *Journal of Aircraft*, Vol. 38, No. 3, 2001, pp. 402-418.
- [3] Gad-el Hak, M., *Flow Control, Passive, Active, and Reactive Flow Management*, Cambridge Univ. Press, Cambridge, England, 2000.
- [4] Anders, S., Sellers, W. L., and Washburn, A., "Active Flow Control Activities at NASA Langley," AIAA Paper 2004-2623, June 2004.
- [5] Tilmann, C. P., Kimmel, R. L., Addington, G., and Myatt, J. H., "Flow Control Research and Application at the AFRL's Air Vehicles Directorate," AIAA Paper 2004-2622, June 2004.
- [6] Miller, D., and Addington, G., "Aerodynamic Flowfield Control Technologies for Highly Integrated Airframe Propulsion Flowpaths," AIAA Paper 2004-2625, June 2004.
- [7] Kibens, V., and Bower, W. W., "An Overview of Active Flow Control Applications at The Boeing Company," AIAA Paper 2004-2624, June 2004.
- [8] Zha, G.-C., and Paxton, D. C., "A Novel Flow Control Method for Airfoil Performance Enhancement Using Co-Flow Jet," *Applications of Circulation Control Technologies*, edited by Joslin, R. D. and Jones, G. S., Progress in Astronautics and Aeronautics, Vol. 214, AIAA, Reston, VA, 2006, pp. 293-314, Chap. 10.
- [9] Zha, G.-C., Carroll, B., Paxton, C., Conley, A., and Wells, A., "High Performance Airfoil with Co-Flow Jet Flow Control," AIAA Paper 2005-1260, Jan. 2005; *AIAA Journal* (submitted for publication).
- [10] Zha, G.-C., Paxton, C., Conley, A., Wells, A., and Carroll, B., "Effect of Injection Slot Size on High Performance Co-Flow Jet Airfoil," *Journal of Aircraft*, Vol. 43, No. 4, July-Aug. 2006, pp. 987-995.
- [11] Zha, G.-C., and Paxton, C., "A Novel Airfoil Circulation Augment Flow Control Method Using Co-Flow Jet," NASA CP-2005-213509, June 2005; also AIAA Paper 2004-2208, June 2004.
- [12] Englar, R. J., "Circulation Control for High Lift and Drag Generation on STOL Aircraft," *Journal of Aircraft*, Vol. 12, No. 5, 1975, pp. 457-463.
- [13] Englar, R. J., Trobaugh, L. A., and Hemmersly, R., "STOL Potential of the Circulation Control Wing for High-Performance Aircraft," *Journal of Aircraft*, Vol. 14, No. 3, 1978, pp. 175-181.

- [14] Liu, Y., Sankar, L. N., Englar, R. J., Ahuja, K. K., and Gaeta, R., "Computational Evaluation of the Steady and Pulsed Jet Effects on the Performance of a Circulation Control Wing Section," AIAA Paper 2004-0056, Jan. 2004.
- [15] Wagnanski, I., "The Variables Affecting the Control Separation by Periodic Excitation," AIAA Paper 2004-2625, June 2004.
- [16] Greitzer, E. M., Tan, C. S., and Graf, M. B., *Internal Flow*, Cambridge Univ. Press, Cambridge, England, 2004.
- [17] Kind, R.-J., "A Proposed Method of Circulation Control," Ph.D. Thesis, Univ. of Cambridge, Cambridge, England, June 1969.
- [18] Jones, G. S., "Pneumatic Flap Performance for a 2D Circulation Control Airfoil, Steady & Pulsed," NASA CP-2005-213509, June 2005; also *Applications of Circulation Control Technologies*, edited by R. D. Joslin and G. S. Jones, Progress in Astronautics and Aeronautics, AIAA, Reston, VA (to be published).
- [19] Wilson, M., and von Kerczek, C., "An Inventory of Some Force Procedure for Use in Marine Vehicle Control," DTNSRDC Paper 791097, Nov. 1979.

R. Lucht  
Associate Editor



***If you are a professional in the field or a student of Aerodynamics, make sure these must-have resources are on your shelf...***

**Introduction to Aeronautics:  
A Design Perspective, Second Edition**

Steven A. Brandt, Randall J. Stiles, John J. Bertin - United States Air Force Academy, and Ray Whitford - Cranfield Institute of Technology

This textbook provides the resources that students need to understand the methods and thought processes involved in designing aircraft. Students learn through the use of specific analytical principles and practical examples taught to them through examples, case studies, and corresponding problems to solve.

**AIAA Education Series**

2004, 510 pages, Hardback

ISBN: 1563477017

**AIAA Member Price: \$74.95**

List Price: \$99.95

**AeroDYNAMIC 3.0**

This Microsoft Windows™ based software package on DVD, titled AeroDYNAMIC, provides a single integrated package with one universal user interface providing access to virtual laboratories, simulations, and design synthesis and analysis software based on the methods presented in

2004, DVD

ISBN: 1563476894

**AIAA Member Price: \$64.95**

List price: \$94.95

**Introduction to Aeronautics and AeroDynamic 3.0 Set**

This set contains Introduction to Aeronautics, Second Edition and AeroDYNAMIC 3.0 DVD.2004, Mixed media

ISBN: 1563476924

**AIAA Member Price: \$79.95**

List Price: \$109.95

To order or for more information contact AIAA by phone: 800/682-2422, fax: 703/661-1595, e-mail: warehouse@aiaa.org or order online at www.aiaa.org.